Laser–Tissue Interaction Modeling with the LATIS Computer Program

R. A. London *M. E. Glinsky*

D. S. Bailey *G. B. Zimmerman*

D. C. Eder

Introduction

The development of new instruments and procedures for use in laser medicine typically involves extensive experimental and clinical studies. Computational modeling of the laser–tissue interaction process can be used to explore and reduce the experimental parameter space (e.g., laser wavelength, pulse length and pulse energy), and to gain a deeper understanding of specific laser-medical processes. In this way, modeling can lead to more rapid development of new instruments and protocols and to the genesis of new ideas. In addition, modeling will be useful in the future for patient-specific treatment planning and for physician training. Modeling will only be useful, however, if it is closely linked to experiments; a project to develop a specific instrument or protocol must involve iteration between modeling and experiment, converging on a set of optimized design parameters. Figure 1 shows a likely iterative process using LATIS, a computer program we have recently developed at the Lawrence Livermore National Laboratory to treat a wide range of laser–tissue interaction phenomena.

The therapeutic uses of lasers fall into three broad classes, depending on the physical mechanism by which the laser interacts with and alters the living tissue: photothermal, photochemical, and photomechanical. The physical processes involved in these three laser–tissue interactions include laser light propagation, thermal heat transport, thermal coagulation, and other material changes; photochemistry; and hydrodynamic motion, respectively. An excellent introduction to many aspects of these processes can be found in a recently published textbook in which chapters have been written by several of the experts in this field.[1] In this article, we present the structure and contents of the LATIS program. We also present a brief discussion of several applications, and a detailed discussion of one application: the problem of laser-light dosimetry with dynamic optical properties.

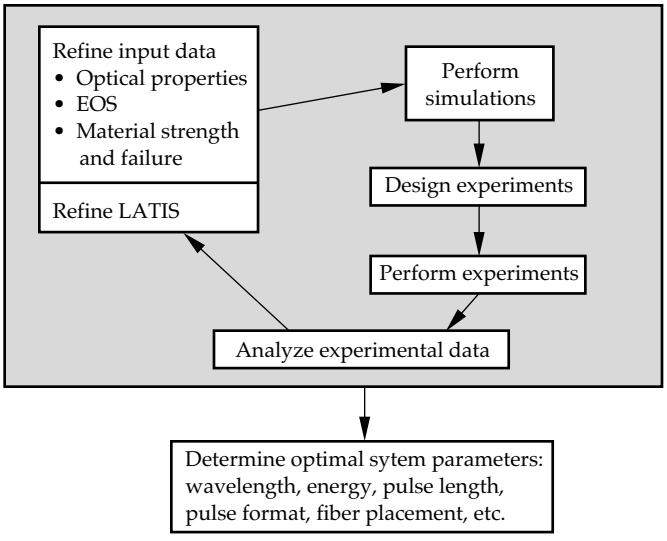

FIGURE 1. LATIS is used in an iterative method along with experiments to design a laser-medicine system. The cycle eventually converges on optimized experiment design parameters. (50-03-0796-1584pb01)

The LATIS Program

LATIS is a two-dimensional, time-dependent simulation program. It is based on the experience gained during 25 years of modeling high-intensity laser–matter interactions for fusion research, particularly with the LASNEX code.[2] LATIS uses cylindrical geometry, with spatial positions described by radial and axial coordinates, r and z. The spatial domain of a calculation is defined by a connected mesh of line segments containing quadrilateral zones. Each line segment intersection is called a mesh point. Positions and velocities are defined at the mesh points, while most material properties, such as temperature and density, are defined at the zone centers. Physical properties are modeled mathematically by analytic formulas, table interpolations, and both ordinary and partial differential equations. Partial differential equations are solved by finite-difference or finite-element methods. In addition, the Monte Carlo method is also used for laser transport, as described below. LATIS is written in

FORTRAN and controlled by a computer-science backplane called Basis.[3] Basis is an interpreter that allows the user considerable flexibility in setting up problems, adding user-defined functions without recompiling the code, and mathematical and graphical post-processing.

The physical processes considered by LATIS are grouped into four categories, as illustrated in Fig. 2: laser propagation, thermal response, material response, and hydro response. For most applications, laser propagation is calculated in the radiation-transfer approximation, although for certain situations, such as ultrashort laser pulses, a wave treatment is needed. Reference 1 describes the radiation transfer approximation in the context of laser–tissue interaction and the associated calculational methods.

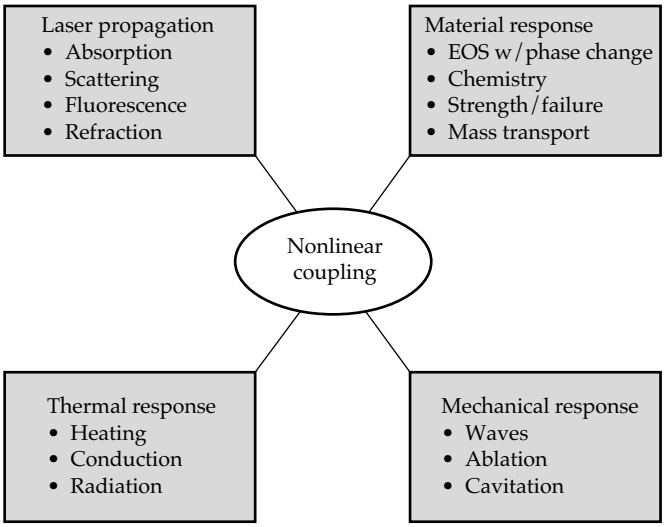

FIGURE 2. LATIS models laser–tissue interactions considering four areas of coupled physical processes. Features such as the hydro response are being developed for future use in tissue ablation applications. (50-03-0796-1585pb01)

Laser Propagation

To model the laser propagation portion of a simulation, we mainly use the time-dependent Monte Carlo method, in which light is represented by a finite number of "super photons"—typically 10^3 to 10^4. Since a typical problem involves on the order of 1 J of laser energy, each super photon represents on the order of 10^{15} real photons. (Henceforth we refer to the super photons simply as photons.) The propagation of the photons is treated in a probabilistic manner. In LATIS, laser photons are created along one or several line segments of the numerical mesh with specified spatial energy distribution and angular distribution relative to the segment normal. A fixed number of photons is introduced at the first time step of the simulation. The photons are then tracked time-dependently through the spatial domain of the calculation. When they cross material interfaces with unequal indices of refraction, such as an air–tissue interface, Fresnel reflection and refraction are calculated. Scattering is calculated probabilistically along a photon's path, according to the scattering coefficient, which may vary in space and time. An anisotropic angular phase function is used to select the scattering angle. We currently use the Henyey–Greenstein phase function, which has been found to be a good approximation to tissue scattering.[4,5] Absorption is calculated analytically along each photon path according to the absorption coefficient, without destroying the photons. Each photon is assigned a weight, which decreases with absorption. When the weight drops below a specified value, typically 1%, the photon is retired from the Monte Carlo calculation. The energy absorbed along the photon path is tabulated in spatial zones, where it is added to the material internal energy. At the end of a time step, a certain number of photons are still "alive" within the spatial domain of the simulation, and a certain number have been removed, either by leaving the domain or by having dropped below the minimum weight. At the beginning of the next time step, new photons are injected if the laser source is still turned on. In order to keep the total number constant at the user-specified value, and to ensure the best statistics, an attempt is made to make the ratio of the number of source photons to the source energy for that particular time step equal to the ratio of the number of living photons to their total energy. If the number of photons that were removed during the time step is not enough to create the desired number of new photons to do this, we use a technique called "combing." Combing reduces the number of photons in zones having two or more photons in a statistical but energy-conserving manner.

In addition to the Monte Carlo method, we have the ablility to invoke the diffusion approximation for laser transport, which is generally faster, but not as accurate near the surface of the material and for complicated geometries. For ultrashort pulses, we are adapting a wave equation solver to calculate the laser propagation and absorption.[6] This is necessary because the absorption occurs via an evanescent wave extending into a high-density plasma, which cannot be described in the radiation transfer approximation.

Thermal Response

Absorption of the laser light primarily goes into raising the tissue temperature according to its specific heat. (For soft tissues this quantity is approximately that of water.) Heat is then carried away from the laser deposition region by thermal conduction and other processes. This is modeled with the well known "bio-heat" equation—essentially a diffusion equation with cooling and heating terms due to blood perfusion and boundary effects (see Refs. 7 and 8 for a basic discussion of the bio-heat equation). The effects of blood perfusion are

important for relatively long pulses (>1 s), which are used mainly for photothermal therapies. Heat exchanges between blood and tissue occurs most effectively in the smallest vessels (the arterioles, venules, and capillaries). In these vessels, the blood and tissue come to the same temperature very rapidly. (In larger vessels, there is little heat transfer between the blood and the tissue due to the rapid flow rate and lower surface-to-volume ratio.) Because the small vessels are generally short (≈1 mm or less) compared to other scales of interest, such as the laser spot size, the blood thermal effects are assumed to be local. By further assuming that the blood coming into the arterioles has a temperature equal to the body core temperature (37°C), we represent the blood–tissue exchange as local heating and cooling rates that are linear in temperature and that drive the tissue towards body temperature. In the models discussed below, we assume specific temperature and damage dependence to the blood perfusion, representing increases due to vessel dilation at slightly elevated temperatures and a decrease due to coagulation at long exposures to high temperature.

Material Response

The material response portion of the LATIS simulation includes calculation of the equation of state (EOS) that specifies the internal energy and pressure of a material as functions of the density and temperature. We usually use steady-state, equilibrium models; however, time-dependent models can be incorporated. It is important to accurately describe phase changes in the EOS, such as the liquid–vapor change in water. In the primary implementation, the EOSs are generated in the form of tables and placed in a simple library format for easy access by LATIS. The tables are produced by the Livermore EOS generator HQEOS,[9,10] which is a global model including solid, liquid, vapor, and plasma states over a wide range of temperatures and densities. Models for chemical processes, such as protein denaturation and tissue coagulation, are included. We have also implemented an "Arrhenius" model, which describes such chemical processes by a single temperature-dependent rate equation.[11] Henceforth these processes are generically called damage. The rate equation is integrated to give a "damage integral"

$$\Omega = \int k\, dt \quad , \tag{1(a)}$$

where the damage rate is

$$k = \frac{k_b T}{h} \exp\left[\frac{\Delta S}{R} - \frac{\Delta H}{RT}\right] \quad . \tag{1(b)}$$

In these equations, k_b, h, and R are the Boltzmann, Planck, and gas constants, T is temperature, and ΔS and ΔH are the entropy and enthalpy of the reaction. This formula applies formally only to ideal first-order reactions. Although in reality the damage processes in tissue are likely to be more complicated, we still use Eq. (1) as a convenient fitting formula to experimental data for such highly temperature-sensitive reactions. The undamaged fraction of the tissue $f_u = \exp(-\Omega)$, while the damaged fraction $f_d = 1 - f_u$. The damage integral is used to alter both the blood perfusion and the scattering coefficient. Other chemical processes, such as those responsible for tissue fusion in a welding procedure or photochemical processes during photodynamic therapy can be modeled in a similar manner. Another set of important material properties are the strength and failure characteristics under mechanical forces. We currently use simple prescriptions, such as a stress-strain relation, but more sophisticated time-dependent models are under development.

Hydrodynamic Response

The fourth category of physical process considered by LATIS is the hydrodynamic response of the tissue. These effects include acoustic waves, elastic and plastic deformations, and large motions such as cavitation and ablation. LATIS solves partial differential equations describing mass and momentum conservation using the Lagrangian method. In this method, the spatial zones represent small mass elements. The mesh points move in response to pressures generated in neighboring zones. The mass stays in each zone, moving with the mesh. The hydro equations are solved by a finite difference method and advanced in time via a second-order differencing scheme. The method is explicit, so that a maximum time step is set by a numerical stability criterion (the "Courant limit"). Other criteria, such as changes in the temperature and density, are also used to set a maximum time step to ensure an accurate and stable solution of the hydro equations.

Coupling

The four areas of interactions are all coupled together allowing for nonlinear effects, such as alteration of the optical and thermal properties by time-dependent variations of temperature. This coupling is done explicitly by the operator splitting method, in which the time advance of each process is calculated using the most recent data from the other processes. The accuracy of this procedure is fixed with time-step controls, ensuring a converged solution.

Applications of LATIS

To date, LATIS has been used to simulate both photothermal and photomechanical laser–tissue interactions. Photochemical applications are planned for future

work in the areas of cancer and arthritis treatment. In the photothermal area, we have used LATIS to study the effects of dynamic optical properties on laser dosimetry[12] (which we summarize below as a detailed example of LATIS in action), welding of intravascular patches,[13,14] and the thermal environment for general tissue welding.[15] In the photomechanical area, we have applied LATIS to study high-precision tissue ablation with ultrashort pulses[16] and laser thrombolysis for stroke therapy.[17]

Laser Dosimetry with Dynamic Optics

Many laser applications are based on raising the temperature of a localized region of tissue for a certain period of time to cause necrosis or other alterations, such as tissue fusion. In these photothermal applications, the local energy dose (energy/unit mass) delivered to the tissue is a critical parameter.

Dynamic optics is defined as the alteration of tissue optical properties by laser irradiation. The effects of dynamic optics on the total dose to the tissue, the size of the damaged region, and the reflected light pattern are very important for photothermal applications of lasers, such as tumor treatments.[18] In this section, we illustrate the application of LATIS to a problem in which the laser scattering coefficient and the blood perfusion change due to thermal damage. We focus on the size of the damage region, and we study how dynamic optics effects vary with the laser-irradiation and tissue parameters.

We chose characteristic, but "generic," tissue properties to demonstrate the capabilities of LATIS and to illustrate the physical effects involving dynamic optics. The optical properties were those of dog myocardium at a laser wavelength of 630 nm. The dynamic scattering coefficient was a linear combination of an undamaged and a damaged coefficient: $\mu_s = \mu_u f_u + \mu_d f_d$, where the tissue f_u and f_d are calculated as described in the paragraph following Eq. (1). The scattering coefficients were $\mu_u = 50\ \text{cm}^{-1}$ and $\mu_d = 350\ \text{cm}^{-1}$. The absorption coefficient was fixed at $\mu_a = 0.3\ \text{cm}^{-1}$. Such parameters are also typical of many other soft tissues in the 630–800-nm range. Thermal properties (heat capacity and conductivity) were taken to be those of water, accurate to 30% for most tissues.[19] Damage rate coefficients were fit to average data for whitening of several tissues: dog prostate, dog heart, and rat and pig liver. The coefficients used in Eq. (1) were $\Delta S = 68.2$ cal/deg/mole and $\Delta H = 45.79$ kcal/mole. With these coefficients, the damage time scale $(1/k)$ varies rapidly with temperature from 100 s at 65°C to 0.5 s at 90°C. In the simulations, the temperature was kept near 72.5°C, at which the damage time scale was 20 s. We also included temperature and damage effects on the blood perfusion.[20] The temperature-dependent coefficient increased linearly by a factor of four between 37°C and 42°C to model increased perfusion due to vessel dilation. It was constant at temperatures above 42°C. The damage-dependent coefficient was an exponential cutoff of the perfusion with the damage integral to account for vessel coagulation.

A standard case was defined with the following parameters: laser pulse length 60 s, laser spot size (radius) = 1 mm, scattering anisotropy factor = 0.9, and blood perfusion rate = 0.4 mL/g/min. The laser irradiation pattern was assumed circular with a constant intensity distribution, and the tissue was assumed initially homogeneous. The irradiation geometry and problem zoning are shown in Fig. 3. Fine zones were placed near the laser spot,

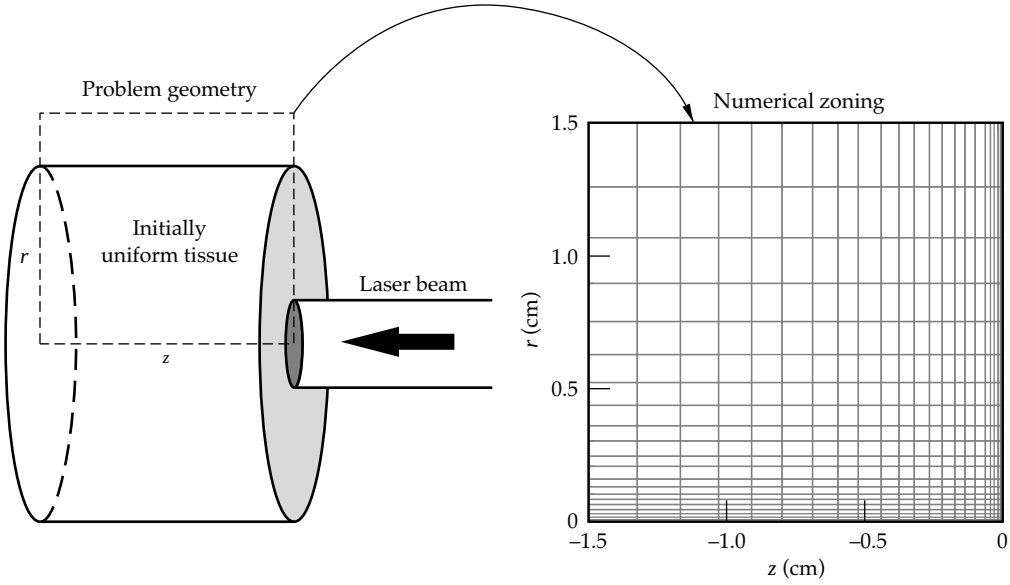

FIGURE 3. The laser–tissue interaction is modeled in cylindrical geometry, with fine zoning near the laser spot and course zones far from the spot. (50-03-0796-1586pb01)

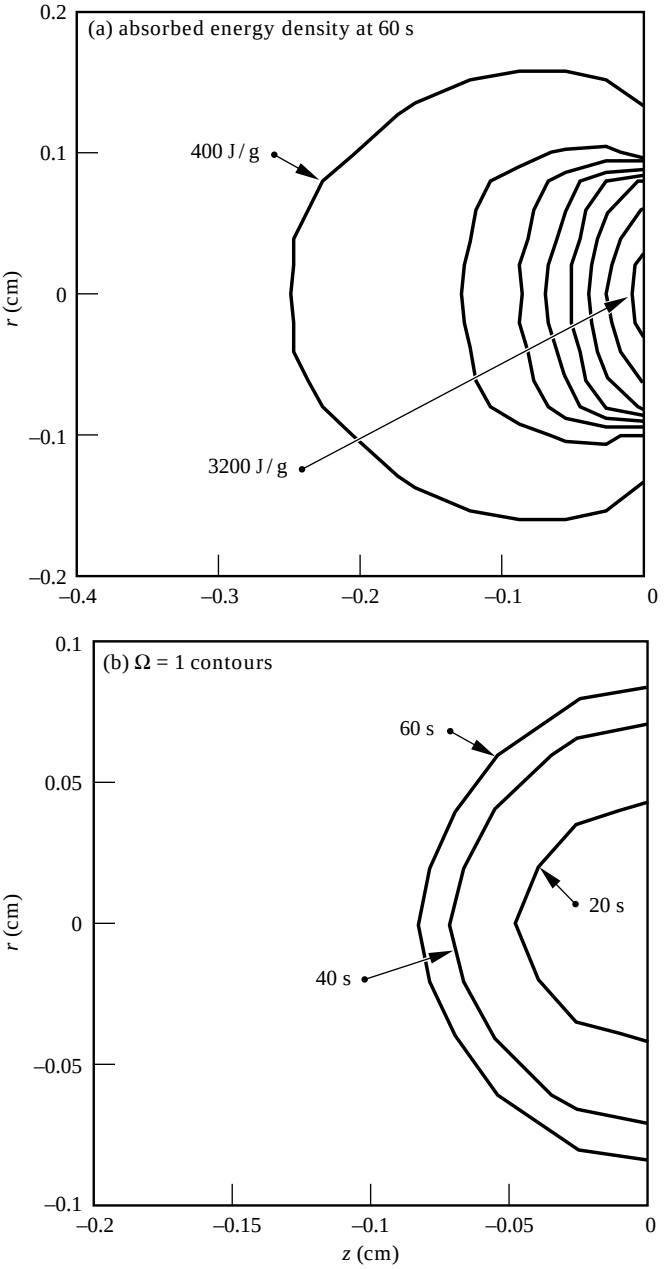

FIGURE 4. The total absorbed energy density integrated over the 60-s pulse is shown in (a). The contour intervals are equal. Laser and tissue conditions are for the standard case. This pattern reflects the light distribution. The damage region ($\Omega = 1$) is shown at various times during the pulse in (b). It grows due to heat diffusion and time-accumulation of damage. (50-03-0796-1587pb01)

where the highest resolution was desired, while courser zones were used far from the laser deposition region. This zoning technique increased the problem resolution while maintaining a relatively small number of zones.

The laser intensity was controlled by a thermostat function that keeps the surface temperature of the directly irradiated region within a desired range. This type of control is motivated by clinical considerations, such as achieving a maximum damage rate over a specified volume without approaching temperatures near 100°C at which tissue dehydration might occur. We actively controlled the laser intensity by monitoring the average temperature in a 3×3 set of tissue zones within the laser spot. We turned the laser off when the temperature exceeded the desired maximum and then turned it back on when the temperature dropped below the desired minimum. We chose a minimum of 70°C and maximum of 75°C. This technique enabled a very good control of the damage progress and avoided adverse effects associated with dehydration or vaporization as temperatures approached 100°C. Such a temperature-control technique has recently been demonstrated experimentally using infrared radiometry by several groups.[21,22]

Results for the distribution of absorbed laser energy and the damage zone for a simulation of the standard case are shown in Figs. 4(a) and 4(b). The absorbed laser light reflects the time-average light distribution, since the absorption coefficient is constant. Due to heat diffusion, the temperature distribution (not shown) extended further from the laser focal region than the laser deposition. The size of the damage zone, as indicated by the $\Omega = 1$ contours of Fig. 4(b), grew in time, due to both heat diffusion beyond the energy deposition region and the increasing time for accumulation of damage.

We now compare the damage zone ($\Omega \geq 1$) for the standard case with dynamic optics to that with static optics in Fig. 5. By static optics we mean a simulation in which the scattering coefficient was kept fixed at its undamaged value even though the tissue became damaged. It is clear that the inclusion of dynamic optics reduces the size of the damage zone. To measure this reduction, we defined a damage ratio as the depth of the damage zone with dynamic optics relative to that without dynamic optics:

$$D \equiv \frac{z(\Omega = 1)\ \text{dynamic}}{z(\Omega = 1)\ \text{static}} \tag{2}$$

For the standard case, as shown in Fig. 5(a), we found $D = 0.67$. For a larger spot size ($r = 0.5$ cm), shown in Fig. 5(b), the effect of dynamic optics was somewhat less than for the standard case—$D = 0.77$.

We performed a parametric study that quantified the reduction in the damage zone caused by dynamic optics. For each parameter variation, we performed two simulations—one with dynamic optical coefficients and one with static coefficients. We then formed the damage ratio as defined above. The parameter variations and resultant damage ratios are listed in Table 1.

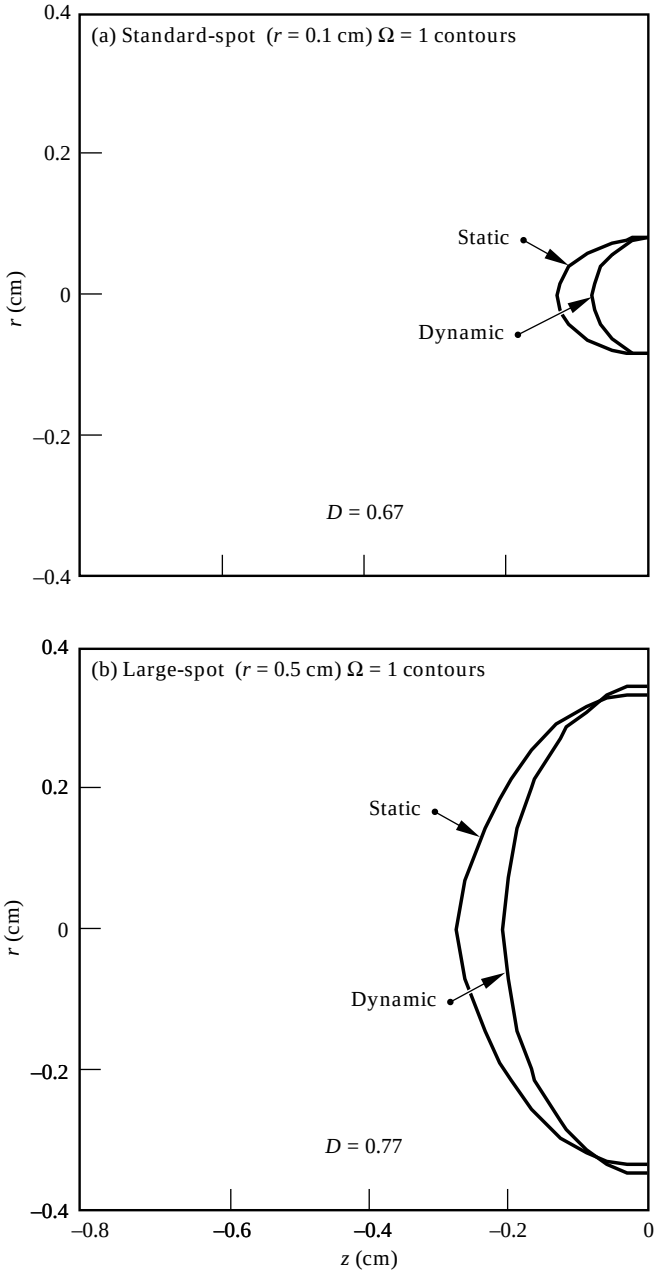

FIGURE 5. The size of the damage regions is reduced by dynamic optics, as shown for the standard case in (a) and for a case with a large spot in (b). The effect of dynamic optics is greater for the standard spot than for the large spot. All curves are for the end of the pulse (at 60 s). (50-03-0796-1588pb01)

The variation with spot size is the greatest. It can be understood by comparing the spot size to the diffusive optical penetration depth $\delta = [3\mu_a(\mu_s + \mu_a)]^{-1/2}$ (see Ref. 1, Chap. 6). For the undamaged tissue, $\delta = 0.46$ cm; for the damaged tissue, $\delta = 0.18$ cm. For spot sizes larger than δ (the case of 0.5 cm spot size), the deposition region is properly given by δ, which scales as $\mu_s^{-1/2}$ for $\mu_s >> \mu_a$ as is the case. For small spot sizes, the laser light scatters out of the beam, leading to smaller deposition region, scaling approximately as μ_s^{-1}. This higher dependence on μ_s leads to the relatively larger effect of dynamic optics for the smaller spots. The variation with pulse length stems from the relationship to the typical damage time scale. We controlled the surface temperature to an average value of 72.5°C, which gave a characteristic damage time scale of 20 s. Thus pulses of about 20 s or less do not have enough time to produce a large damage zone and therefore show less difference between the dynamic optics and the static optics cases as indicated in Table 1. We also explored variations in the isotropy of scattering and the blood perfusion rate. The isotropic scattering case assumed smaller scattering coefficients, so that the "reduced scattering coefficient" $\mu_s' = \mu_s(1 - g)$ was the same as for the standard case with $g = 0.9$. This was found to have very little effect on the simulation results. The case with no blood perfusion showed 10% larger damage depth in both dynamic and static cases, but very little differential effect, as seen in Table 1.

TABLE 1. Parameter variations and corresponding damage ratios.

Parameter variation	Damage ratio
Standard case	0.67
Short pulse (20 s)	0.76
Long pulse (180 s)	0.63
Small spot (0.01 cm)	0.39
Large spot (0.5 cm)	0.77
Isotropic scattering	0.67
No blood perfusion	0.66

In summary we see that dynamic optics reduces the depth of damage by about 33% in most cases, with the greatest sensitivity to the irradiation spot size and pulse length. This study illustrates the importance of including such nonlinear effects in designing protocols for laser thermotherapies. Projects on thermotherapy for benign prostate hyperplasia and laser–tissue welding are currently in progress in which similar modeling is being used to design experiments and to compare directly with measured data.

Summary

The LATIS computer program is being developed to treat all of the important aspects of laser–tissue interaction including laser propagation, thermal effects, material effects, and hydrodynamics, in a fully coupled manner. In LATIS, we now have a powerful tool for designing new medical devices and procedures through computational simulation. LATIS is being applied to areas of photothermal therapy, tissue welding, hard-tissue ablation, and thrombolysis.

Notes and References

1. A. J. Welch and M. J. C. Van Gemert, *Optical-Thermal Response of Laser-Irradiated Tissue* (Plenum Press, New York, 1995).
2. G. B. Zimmerman and W. L. Kruer, *Commun. Plasma Phys. Controlled Fusion* **11**, 82 (1975).
3. P. F. DuBois, *Computers in Physics* **8**, 70 (1994).
4. L. G. Henyey and J. L. Greenstein, *Astrophys. J.* **93**, 70 (1941).
5. S. L. Jacques, C. A. Alter, and S. A. Prahl, *Lasers Life Sci.* **1**, 309 (1987).
6. W. E. Alley, *A Maxwell equation solver for the simulation of moderately intense ultra-short pulse laser experiments*, p. 160, UCRL-LR-105820-92, Lawrence Livermore National Laboratory, Livermore, CA (1992).
7. Y. I. Cho, ed., "Bioengineering Heat Transfer," *Advances in Heat Transfer*, vol. 22 (Academic, San Diego, 1992).
8. C.-S. Orr and R. C. Eberhart, *Optical-Thermal Response of Laser-Irradiated Tissue*, p. 367, A. J. Welch and M. J. C. Van Gemert, Eds., Plenum Press, New York, 1995.
9. R. M. More, K. H. Warren, D. A. Young, and G. B. Zimmerman, *Phys. Fluids* **31**, 3059 (1988).
10. D. A. Young and E. M. Corey, *J. Appl. Phys.* **78**, 3748 (1995).
11. J. Pearce and S. Thomsen, *Optical-Thermal Response of Laser-Irradiated Tissue*, p. 561, A. J. Welch and M. J. C. Van Gemert, Eds., Plenum Press, New York, 1995.
12. R. A. London, M. E. Glinsky, G. B. Zimmerman, D. C. Eder, and S. L. Jacques, *Laser-Tissue Interaction VI* (SPIE—The International Society for Optical Engineering, Bellingham, WA, 1995; *Proc. SPIE* **2391**), p. 431.
13. M. E. Glinsky, R. A. London, G. B. Zimmerman, and S. L. Jacques, *Laser-Tissue Interaction VI* (SPIE—The International Society for Optical Engineering, Bellingham, WA, 1995; *Proc. SPIE* **2391**), p. 262.
14. M. E. Glinsky, R. A. London, G. B. Zimmerman, and S. L. Jacques, *Medical Applications of Lasers III* (SPIE—The International Society for Optical Engineering, Bellingham, WA, 1996; *Proc. SPIE* **2623**), p. 349.
15. D. J. Maitland, D. C. Eder, R. A. London, M. E. Glinsky, and B. A. Soltz, *Lasers in Surgery: Advanced Characterization, Therapeutics, and Systems VI* (SPIE—The International Society for Optical Engineering, Bellingham, WA, 1996; *Proc. SPIE* **2671**), p. 234.
16. R. A. London et al., *Laser–Tissue Interaction VII*, Ed. S. L. Jacques, *Proc. SPIE* **2681**, Bellingham WA, 1996, p. 233.
17. M. Strauss et al., *Lasers in Surgery: Advanced Characterization, Therapeutics, and Systems VI*, (SPIE—The International Society for Optical Engineering, Bellingham, WA, 1996; *Proc. SPIE* **2671**), p. 11.
18. G. Muller and A. Roggan, *Laser-Induced Interstitial Thermotherapy* (SPIE—The International Society for Optical Engineering, Bellingham, WA, 1995; *Proc. SPIE*).
19. J. W. Valvano, *Optical-Thermal Response of Laser-Irradiated Tissue*, p. 445, A. J. Welch and M. J. C. Van Gemert, Eds., Plenum Press, New York, 1995.
20. B.-M. Kim, S. L. Jacques, S. Rastegar, S. L. Thomsen, and M. Motamedi, *Laser-Tissue Interaction VI* (SPIE—The International Society for Optical Engineering, Bellingham, WA, 1995; *Proc. SPIE* **2391**), p. 443.
21. B. Lobel et al., *Lasers in Surgery: Advanced Characterization, Therapeutics, and Systems V* (SPIE—The International Society for Optical Engineering, Bellingham, WA, 1995; *Proc. SPIE* **2395**), p. 517.
22. I. Cilesiz, E. K. Chan, A. J. Welch, and S. L. Thomsen, *Lasers in Surgery: Advanced Characterization, Therapeutics, and Systems V* (SPIE—The International Society for Optical Engineering, Bellingham, WA, 1995; *Proc. SPIE* **2395**), p. 523.